

TITLE

Corona and Influenza Virus Proteolytic Priming takes place in Tetraspanin-Enriched Membrane Microdomains

RUNNING TITLE

Virus priming in TEMs

AUTHORS

James T. Earnest, Michael P. Hantak, Jung-Eun Park, Tom Gallagher*

AFFILIATIONS

Department of Microbiology and Immunology

Loyola University Medical Center

2160 South First Avenue

Maywood, IL, 60153, USA

*tgallag@luc.edu

1 **ABSTRACT**

2 Coronaviruses (CoVs) and low-pathogenicity influenza A viruses (LP IAVs) depend on
3 target cell proteases to cleave their viral glycoproteins and prime them for virus-cell
4 membrane fusion. Several proteases cluster into tetraspanin-enriched microdomains
5 (TEMs), suggesting that TEMs are preferred virus entry portals. Here we found that
6 several CoV receptors and virus-priming proteases were indeed present in TEMs. Isolated
7 TEMs, when mixed with CoV and LP IAV pseudo-particles, cleaved viral fusion proteins to
8 fusion-primed fragments and potentiated viral transductions. That entering viruses utilize
9 TEMs as a protease source was further confirmed using tetraspanin antibodies and
10 tetraspanin shRNAs. Tetraspanin antibodies inhibited CoV and LP IAV infections, but their
11 virus-blocking activities were overcome by expressing excess TEM-associated proteases.
12 Similarly, cells with reduced levels of the tetraspanin CD9 resisted CoV pseudo-particle
13 transductions, but were made susceptible by overproducing TEM-associated proteases.
14 These findings indicated that antibodies and CD9 depletions interfere with viral proteolytic
15 priming, in ways that are overcome by surplus proteases. TEMs appear to be exploited by
16 some CoVs and LP IAVs for appropriate co-engagement with cell receptors and proteases.

17 **IMPORTANCE**

18 Enveloped viruses use their surface glycoproteins to catalyze membrane fusion, an
19 essential cell entry step. Host cell components prime these viral surface glycoproteins to
20 catalyze membrane fusion at specific times and places during virus-cell entry. Amongst
21 these priming components are proteases, which cleave viral surface glycoproteins,
22 unleashing them to refold in ways that catalyze virus-cell membrane fusions. For some

23 enveloped viruses, these proteases are known to reside on target cell surfaces. This
24 research focuses on corona- and influenza A- virus-cell entry, and identifies TEMs as sites
25 of viral proteolysis, thereby defining subcellular locations of virus priming with greater
26 precision. Implications of these findings extend to the use of virus entry antagonists, such
27 as protease inhibitors, which might be most effective when localized to these
28 microdomains.

29 INTRODUCTION

30 Enveloped viruses require fusion with host cell membranes to deliver viral genetic
31 material and initiate infection. This process is catalyzed by fusion glycoproteins, which
32 project from virion membranes and operate by bringing virion and host cell membranes
33 into proximity, ultimately stimulating their coalescence. Amongst the host cell factors
34 required for this membrane fusion are receptors and proteases. Receptors tether viruses
35 to host cell membranes and proteases cleave fusion protein precursors to form the
36 domains that catalyze membrane melding. This proteolytic step is termed “priming”, and
37 depending on the virus type, may take place in virus-producing cells (1), in extracellular
38 environments (2), or in virus-target cells (3). Notably, several protease inhibitors prevent
39 viral fusion protein cleavages, and as such, are antiviral agents (4).

40 For many respiratory viruses, including several coronaviruses (CoVs) and low
41 pathogenic (LP) influenza A viruses (IAVs), the relevant priming proteases operate in virus-
42 target cells. These proteases cleave the virion glycoproteins mediating receptor binding
43 and membrane fusion, namely the spike (S) proteins for CoVs and the hemagglutinin (HA)
44 proteins for IAVs. These proteases include type II transmembrane serine proteases

45 (TTSPs), a relatively large family of plasma membrane – localized glycoproteins that
46 proteolyze numerous extracellular substrates (5). Specifically, the TTSP member
47 Transmembrane Protease Serine 2 (TMPRSS2) primes CoVs, including Severe Acute
48 Respiratory Syndrome (SARS)-CoV (6, 7) and Middle East Respiratory Syndrome (MERS)-
49 CoV (8, 9). Without TMPRSS2, target cells are significantly less sensitive to these CoVs (8,
50 10), but they are not entirely CoV-resistant, as other host proteases, i.e., cathepsins, can
51 provide for some priming (11, 12). TMPRSS2 and the TTSP human airway trypsin-like
52 (HAT) protease are also sufficient to prime LP IAV, both *in vitro* (13) and *in vivo* (14). As
53 there is no evidence for cathepsin priming of IAVs, cell-surface proteases may be strictly
54 required to prime LP IAV (15).

55 The requirement for TTSP-mediated proteolytic processing of CoV and LP IAV
56 glycoproteins is established, but the subcellular location of these cleavage events is not well
57 understood. If these proteases operate during virus entry, then it is likely that target-cell
58 virus receptors would co-reside with priming proteases to make virus priming feasible (7).
59 One possible location for this co-residence is within tetraspanin-enriched microdomains
60 (TEMs). TEMs are comprised of homo- and hetero-typic assemblies of tetraspanins, so
61 named for their four-transmembrane spanning architectures. In TEMs, the tetraspanins
62 form a locally-ordered, largely plasma membrane-embedded platform in which projecting
63 integral-membrane adhesion receptors and enzymes are interspersed. As dynamically
64 organized membrane protein complexes, TEMs function to modulate cell adhesion,
65 migration and differentiation (16, 17) as well as pathogen invasion (18).

66 There is some modest support for the hypothesis that CoV and LP IAV receptors and
67 proteases are concentrated in TEMs, and that priming of these viruses is therefore highly
68 localized. First, TEMs contain CoV receptors dipeptidyl-peptidase 4 (DPP4) (19) and
69 aminopeptidase N (APN) (20), and also contain sialic acids (21), the receptors for IAVs.
70 Second, TEMs contain a variety of integral membrane proteases (22). Third, IAV cell entry
71 is both preferentially observed at CD81 tetraspanin-enriched endosomal locations (23) and
72 reduced by CD81 depletion (24).

73 Since some CoV receptors interact with tetraspanins, and since LP IAV infection was
74 reduced by tetraspanin CD81 knockdown, we used both CoVs and IAVs to address the
75 importance of TEMs in cell entry. We evaluated the effects of tetraspanin antibodies and
76 individual CD9 tetraspanin depletion on virus-cell entry. We isolated TEMs and analyzed
77 them for the presence of virus receptors and virus-priming proteases. We used the isolated
78 TEMs to extracellularly prime CoVs and IAVs. Our findings supported the hypothesis that
79 these enveloped viruses enter cells through TEMs because these microdomains harbor
80 both virus receptors and virus-priming proteases.

81 **MATERIALS AND METHODS**

82 **Cells.** Human embryonic kidney HEK cells 293T and 293 β 5 (25) and MDCK cells were
83 maintained in Dulbecco's modified Eagle's medium (DMEM) (Thermo Scientific)
84 supplemented with 10% fetal bovine serum (FBS; Atlanta Biologicals), 1X non-essential
85 amino acids, 10 mM HEPES, 1 mM sodium pyruvate, and 100 U/ml penicillin-streptomycin
86 solution (Thermo Scientific). DBT cells were maintained in minimal essential media (MEM)
87 supplemented with 10% tryptose phosphate broth, 5% FBS, 100 U/ml penicillin-

88 streptomycin, and 2 mM L-glutamine. Cells were maintained in a humidified environment
89 at 37°C and 5% CO₂.

90 **Plasmids.** Codon-optimized MERS S containing sequences for a C-terminal C9 epitope tag
91 was purchased from Genscript and subsequently cloned into pcDNA3.1+ between the *EcoRI*
92 and *NotI* restriction sites. pcDNA3.1-229E-S-C9 and pcDNA3.1-hAPN plasmids were
93 provided by Dr. Fang Li, University of Minnesota. pcDNA3.1-SARS-S-C9 and pcDNA3.1-
94 ACE2-C9 plasmids were provided by Dr. Michael Farzan, Scripps Research Institute.
95 pcDNA3.1-HA5-QH-trypsin site was provided by Dr. Lijun Rong, University of Illinois-
96 Chicago, and is previously described (26). The pHEF-VSV-G plasmid was obtained from BEI
97 Resources. pcDNA3.1-murine carcinoembryonic antigen-related cell adhesion molecule
98 (mCEACAM) was described previously (27). C-terminal FLAG-tagged human DPP4 plasmid
99 pCMV6-Entry-hDPP4 (NCBI Reference Sequence [NM_001935](#)) was purchased from
100 OriGene. pCAGGS-TMPRSS2-FLAG and pCAGGS-TMPRSS2-S441A-FLAG were previously
101 constructed (7). TMPRSS11D (HAT) was obtained from Open Biosystems and cloned into
102 pCAGGS between *SacI* and *XhoI* restriction sites. pCMVSPORT6-human CD9 was purchased
103 from Open Biosystems. CD9 and scramble control shRNA constructs flanked by the U6
104 promoter and a RNA Polymerase III stop sequence were engineered into the pUC57 vector
105 by Genscript. The pNL4.3-HIVluc plasmid was provided by the NIH AIDS Research and
106 Reference library. pΔEGFP-S15-mCherry (28) was provided by Dr. Edward Campbell,
107 Loyola University Chicago. pEGFP was provided by Dr. Chris Wiethoff, Loyola University
108 Chicago.

109 **Antibodies.** Monoclonal mouse antibodies against CD9 (clone M-L13), CD63 (clone H5C6),
110 and CD81 (clone JS-81) were obtained from BD Pharmingen. Rabbit anti-FLAG and anti- β -
111 actin-HRP antibodies were obtained from Sigma Aldrich. Mouse anti-rhodopsin (C9)
112 antibodies were obtained from Millipore. Rabbit anti-CD13 (APN) antibodies were
113 obtained from Abcam. Mouse anti-calnexin antibodies were obtained from Cell Signaling.
114 A mouse monoclonal antibody to IAV H1 HA (clone PY102) was provided by Dr. Balaji
115 Manicassamy, University of Chicago. Secondary antibodies were purchased from
116 Invitrogen and include goat-anti-rabbit-AlexaFluor 488, goat-anti-mouse-AlexaFluor 488,
117 and goat-anti-mouse-AlexaFluor 568. Donkey-anti-goat, goat-anti-mouse, and goat anti-
118 rabbit HRP conjugated antibodies were purchased from Thermo Scientific.

119 **Viruses.** Influenza A/Puerto Rico/8/1934 H1N1 (PR8) containing a *Gaussia* luciferase
120 (Gluc) reporter gene (29) was provided by Dr. Peter Palese, Mount Sinai School of
121 Medicine. PR8-Gluc stocks were produced using a standard protocol (30). Briefly, MDCK
122 cells were inoculated with PR8-Gluc, and incubated in DMEM supplemented with 0.2%
123 BSA. 30 hours post infection (hpi), progeny were collected, treated with TPCK-trypsin
124 (Sigma), and used to infect fresh MDCK cells at MOI =1. Supernatants were then collected,
125 clarified by centrifugation, aliquoted and stored at -80°C. Two strains of recombinant
126 mouse hepatitis viruses (MHV), MHV-A59 and MHV-JHM, each containing a firefly
127 luciferase (Fluc) reporter gene, were produced and titered on DBT cells as described
128 previously (31).

129 **Pseudoviruses.** VSV – based pseudovirus particles (pp) were produced by the methods of
130 Whitt, 2010 (32). Briefly, 293T cells were transfected with plasmids encoding indicated

131 viral glycoproteins. Two days later, cells were inoculated for 2 h with VSVΔG-luciferase
132 (32), rinsed extensively and incubated for one day. Supernatants were collected,
133 centrifuged at 800 x g for 10 min to remove cellular debris, and stored in aliquots at -80°C.
134 HIV – based pp were produced as previously described (28). Briefly, 293T cells were co-
135 transfected with pNL4.3-HIV-luc and pcDNAs encoding appropriate glycoproteins, and
136 where indicated, pΔEGFP-S15-mCherry was also co-transfected. After two days,
137 supernatants were collected, centrifuged at 1,000 x g at 4°C for 10 min to remove cell
138 debris, and stored in aliquots at -80°C.

139 **CD9 knockdowns.** Two shRNA constructs were used, one designed to target CD9 and the
140 other a scrambled control. 293β5 cells were co-transfected with 0.05 μg/10⁶ cells of
141 pCDNA3.1-hDPP4 along with 1 μg/10⁶ cells of the indicated shRNA plasmid or a pUC57
142 construct lacking the shRNA. Stable transfectants were selected in DMEM-10% FBS
143 containing 1.2 mg/mL of G418 (Thermo Scientific), for the neomycin resistance on the
144 DPP4 plasmid. Cells underwent selection for at least 7 days before being used in assays.

145 **Infection in the presence of tetraspanin antibodies.** DBT cells or 293β5 cells were
146 transfected with appropriate plasmids encoding viral receptors or proteases, divided into
147 96-well cluster plates, and incubated for 30 min at 37°C with indicated antibodies, at 0.12
148 μg/μl (~10⁷ antibodies / cell). Indicated viruses were then added for 2 h at 37°C, then cells
149 were rinsed, incubated at 37°C for 6 h (MHV and PR8), 16 h (VSV), or 48 h (HIV). For PR8,
150 cells were not lysed, and media were analyzed for secreted Gluc. For the other viruses,
151 cells were lysed in passive lysis buffer (Promega). Luciferase levels in media or lysates

152 were measured after addition of either Fluc substrate (Promega) or Gluc substrate (New
153 England Biolabs) using a Veritas microplate luminometer (Turner BioSystems).

154 **Flow Cytometry.** To measure antibody binding, 293β5 cells were lifted with Accutase
155 (Millipore), pelleted and resuspended to 10⁶ cells/ml in phosphate buffered saline (PBS)
156 supplemented with 2% FBS containing indicated antibodies at 0.12 μg/μl. After 30 min at
157 37°C, cells were rinsed thrice by pelleting and resuspension in PBS-2% FBS, then incubated
158 for 30 min at 4°C with AlexaFluor 488 – conjugated donkey-anti-mouse IgG. After
159 sequential rinsing, cell fluorescence was detected using a BD C6 Accuri flow cytometer. To
160 measure HIV pp binding, 293β5 cells, transfected with empty pCMV6 or with pCMV6-
161 Entry-hDPP4, were suspended in PBS-2% FBS. Cells were divided and aliquots were
162 incubated for 30 min at 37°C with tetraspanin antibodies at 0.12 μg/μl. Cells were chilled,
163 then incubated for 1h on ice with HIV-mCherry-MERS S. Cells were rinsed thrice by
164 pelleting and resuspension, and mCherry fluorescence detected using a BD C6 flow
165 cytometer or a BD LSRFortessa flow cytometer, as indicated. All flow cytometric data were
166 analyzed using FlowJo software.

167 **Fluorescence activated cell sorting.** DBT cells were transfected with 0.5 μg of pEGFP, and
168 a total of 4 μg of a pCAGGS empty vector or TMPRSS2 plasmid per 10⁶ cells. 24 h after
169 transfection, cells were lifted with trypsin, washed 3 times with cold PBS supplemented
170 with 2% FBS, and sorted using a BD FACSAria cell sorter. Live, GFP⁺ cells were plated and
171 incubated at 37°C overnight before antibody blockade experiments were performed as
172 described above.

173 **Immunofluorescence microscopy.** 293β5 cells were transfected with indicated plasmid
174 DNAs, incubated for two days, and then cooled to room temperature (RT). Antibodies and
175 HIV-mCherry pps were added, cells incubated for 30 min at RT, 10 min at 37°C, then
176 returned to RT. AlexaFlour – conjugated secondary antibodies were applied for 10 min at
177 RT, along with Hoechst 33258 (Molecular Probes). Cells were rinsed with PBS, fixed with
178 3.7% paraformaldehyde in 100 mM PIPES buffer [pH 6.8], mounted using PermaMount,
179 and imaged with a DeltaVision microscope (Applied Precision) equipped with a digital
180 camera (CoolSNAP HQ; Photometrics), using a 1.4-numerical aperture 60X objective lens.
181 Images were deconvolved with SoftWoRx deconvolution software (Applied Precision). Co-
182 localization was measured and quantified using Imaris version 6.3.1 (Bitplane Scientific
183 Solutions).

184 **Isolation of Tetraspanin-Enriched Microdomains (TEMs).** Adherent 293β5 cells (~10⁵ /
185 cm²) were rinsed with ice-cold PBS, incubated for 30 min at 4°C with 1 mg / ml EZ-Link
186 Sulfo-NHS-LC-Biotin (Pierce) in PBS, rinsed, then incubated for 20 min at 4°C with 100 mM
187 glycine in PBS. Cells were rinsed with PBS, then incubated for 20 min at 4°C in MES buffer
188 (25 mM MES [pH 6.0], 125 mM NaCl, 1 mM CaCl₂, 1 mM MgCl₂) containing 1% 3-[(3-
189 Cholamidopropyl)dimethylammonio]-1-propanesulfonate (CHAPS) detergent (Calbiochem
190 Cat # 220201) or 1% TritonX-100 detergent (Sigma). Cell lysates (10⁷ / ml) were removed
191 from plates and emulsified by 20 cycles of extrusion through 27G needles. Nuclei were
192 removed by centrifugation, lysates mixed with equal volumes of 80% w/v sucrose in MES
193 buffer, placed into Beckman SW60 tubes, and overlaid with 3 ml of 30% w/v sucrose, then
194 with 0.5 ml of 5% w/v sucrose, both in MES buffer. Samples were centrifuged with a
195 Beckman SW60 rotor at 370 K x g for 18 h at 4°C. Fractions were collected from air-

196 gradient interfaces. Biotinylated proteins in gradient fractions were bound to streptavidin
197 agarose beads (Pierce). Non-reducing dot- and western-blotting procedures were used to
198 identify the distributions of proteins in gradient fractions, as described previously (33).

199 ***Virus priming assays.*** PR8 or MERS pp were incubated at 37°C for 30 min with equal
200 volumes of low-density (LD) or high-density (HD) sucrose gradient fractions, or with 2.5 U
201 trypsin / reaction (in 50 µl total) (Sigma). Treated PR8 and MERS pp were divided, and
202 proteins in one set of aliquots were precipitated with trichloroacetic acid and analyzed by
203 western blotting. The other set were used to transduce 293β5 cells. Cells transduced with
204 MERS pp were pre-treated for 1h with or without 10 µM leupeptin (Sigma), inoculated for
205 2 h, rinsed and incubated without leupeptin for 18 h. Cells were then lysed and luciferase
206 levels were measured. Cells infected with PR8 viruses were infected at an MOI=1, rinsed
207 after 2 h, and incubated for an additional 6 h. Media were collected and Gluc levels were
208 measured.

209 **RESULTS**

210 ***Tetraspanin antibodies inhibit coronavirus and influenza A virus infections.***

211 Tetraspanins facilitate the entry of many viruses, including hepatitis C (34), human
212 papilloma (35), and IAV (23). To determine whether entering CoVs also utilize
213 tetraspanins, we evaluated the effects of tetraspanin antibodies on infection by mouse
214 hepatitis virus (MHV) strains A59 and JHM. To this end, murine DBT cells were incubated
215 for 30 min with mouse monoclonal antibodies against the tetraspanins CD9, CD63, CD81, or
216 with an equimolar mixture of the three (αTspan). A monoclonal antibody against
217 transferrin receptor (TfR) was used as an isotype - matched control for general cell coating

218 by antibodies. Cells were inoculated with luciferase-expressing recombinant MHV-A59 or –
219 JHM for 2 h, then unadsorbed viruses and antibodies were rinsed away. As measured by
220 luciferase levels at 8 hpi, the two viruses were significantly inhibited by all three
221 tetraspanin antibodies, with the antibody combination (α Tspan) inhibiting A59 and JHM
222 strains by ~50% and ~90% , respectively (Fig. 1A). The TfR antibodies did not block the
223 viruses. None of the antibodies interfered with transduction by VSV pps bearing VSV G
224 proteins (VSV pp), indicating that tetraspanin antibodies do not generally suppress virus
225 entry or reporter gene expression.

226 While previous studies have found that CD81 knockdown inhibits IAV entry (23), it
227 is not known whether antibodies to CD81 or other tetraspanins also inhibit IAV infection.
228 Thus we determined whether the tetraspanin antibodies inhibit influenza A/Puerto
229 Rico/8/1934 (H1N1), also known as PR8 IAV. For ease of analysis, we used PR8 containing
230 a *Gussia* luciferase (Gluc) reporter gene (29). Many host cells are resistant to PR8
231 infection, because they do not express proteases that prime viral HA proteins (13).
232 Therefore, we transfected 293 β 5 cells with plasmids encoding HAT or TMPRSS2, then
233 infected with PR8 one day later. HAT will make target cells susceptible to LP-IAV, while
234 TMPRSS2 will not (15). By measuring Gluc accumulations in culture media, we determined
235 that transfecting cells with 0.001 μ g/well of HAT was sufficient to render cells susceptible
236 to PR8 infection and that increasing HAT transfection generally led to increased infection
237 (Fig. 1B). Knowing this, we determined whether tetraspanin antibodies might block PR8
238 infection of the HAT-expressing cells. Indeed PR8 infection was significantly inhibited by
239 all three tetraspanin antibodies, with the antibody combination (α Tspan) effecting ~ 50%
240 blockade. The tetraspanin antibodies did not inhibit VSV pp transductions (Fig. 1C).

241 ***Tetraspanin antibodies inhibit coronaviruses at the cell entry stage.*** To limit our
242 analyses of tetraspanin antibodies to single-cycle infections, we produced several VSV-
243 based pps, each encoding Fluc reporter genes and each containing the S proteins of a
244 relevant human CoV. The virus preparations were designated according to their S proteins
245 (MERS pp, SARS pp, 229E pp). Their transduction into cells was taken to reflect features of
246 the authentic MERS, SARS and 229E CoV entry processes (7, 33). Transduction-susceptible
247 target cells were established by transfecting 293 β 5 cells with genes encoding virus
248 receptors: hAPN for HCoV-229E (36), hDPP4 for MERS-CoV (37), and hACE2 for SARS-CoV
249 (38). These target cells were then inoculated with the pp preparations, in the absence or
250 presence of tetraspanin antibodies, as was done with authentic viruses. After 1h
251 inoculation periods, unadsorbed pps and antibodies were removed, and transduction levels
252 measured the next day by quantifying Fluc gene expressions.

253 The tetraspanin antibodies impaired transductions by all three CoV pps, with MERS
254 pp and SARS pp most notably inhibited (Fig. 2A). TfR antibodies did not affect
255 transductions. Using MERS pps, we further determined that tetraspanin antibodies were
256 inhibitory only at the pp entry stage, with no effects on transduction when added 30 min
257 following virus inoculation (Fig. 2B). Furthermore, inhibition by the tetraspanin antibodies
258 was not related to the viral particle core, as HIV-based MERS pps were blocked equally to
259 VSV-based MERS pps (data not shown). All of these findings were consistent with
260 inhibition of virus entry at TEMs.

261 ***Tetraspanin antibodies do not block virus-cell binding.*** To determine whether
262 the antibodies used for virus blockades bound similarly to target cells, we subjected

263 antibody-coated cells to flow cytometry. The inert TfR antibodies and inhibitory
264 tetraspanin antibodies bound similarly (Fig 3A), indicating that virus blockades do not
265 arise simply from high levels of antibodies on cells. Next, to determine whether antibodies
266 on cells interfere with virus-cell binding, we used fluorescently-labeled, HIV-based MERS
267 pps, which we manufactured according to prescribed methods (28). mCherry MERS pps
268 were adsorbed at 4°C to 293β5 cells overexpressing hDPP4 receptors, either in the absence
269 or presence of tetraspanin antibodies. Subsequent flow cytometric analyses revealed that
270 the fluorescent HIV-based MERS pps bound abundantly to the ~35% of cells that were
271 overexpressing hDPP4 (Fig. 3B, left). Tetraspanin antibodies did not reduce this
272 percentage of cells bound by MERS pp, (Fig. 3B, right). Tetraspanin antibodies did slightly
273 reduce the fluorescence intensities of the MERS pp-bound cells (Fig. 3B, compare left red
274 and right gold lines). We conclude that the tetraspanin antibodies only modestly interfered
275 with virus binding to cells.

276 These data strongly suggested that tetraspanin antibodies interfere with virus entry
277 after virus-receptor binding. To explain how the antibodies block viruses, we posited that
278 viruses might associate with TEMs after binding to cells, and that the tetraspanin
279 antibodies disrupt some TEM-associated process(es) facilitating virus entry. To determine
280 whether the mCherry MERS pps do indeed appear at TEMs during their cell entry, we
281 incubated chilled 293β5 cells with the fluorescent pps along with tetraspanin CD81
282 antibodies, then shifted to 37°C for 10 min to permit “patching”, i.e., antibody-mediated
283 tetraspanin cross-linking into larger TEM structures (39). Quantitative confocal
284 microscopy revealed that CD81 colocalized with ~20% of MERS pps, but with only ~10%
285 of VSV pps (Fig. 3C, right). Absence of “bald”, i.e. viral glycoprotein-free fluorescent pp

286 binding (Fig. 3C, left) confirmed viral glycoprotein-dependent interactions with cells.
287 Similar, but less compelling co-patching of IAV pp and CD81 were also observed in these
288 experiments (Fig. 3C). These data indicate that, shortly after binding to cells, some MERS
289 and IAV pp will be present at TEM locations.

290 ***Proteases eliminate the antiviral activities of tetraspanin antibodies.*** TEMs are
291 known to contain a variety of cell-surface proteases (22), among which may be one or
292 several CoV and IAV -priming proteases (7, 8, 13, 14). This led us to hypothesize that
293 tetraspanin antibodies interfere with TEM-associated proteolytic priming, possibly by
294 preventing TEM proteases from accessing receptor-bound viruses. By this hypothesis,
295 overexpression of proteases, or addition of proteases to media, should provide viral access
296 to priming and thereby reduce or eliminate the antiviral activities of the tetraspanin
297 antibodies. Thus we overexpressed priming proteases in target cells and performed
298 antibody blockade experiments. Using the frequently-cited CoV priming protease
299 TMPRSS2 (8, 40), we found that MHV infections into DBT cells were augmented ~ 20-fold
300 by TMPRSS2 overexpression, indicating that this protease is utilized by MHV and is limiting
301 in the DBT cell context. We supplied DBT cells with graded doses of TMPRSS2 – encoding
302 plasmids, along with small constant amounts of a GFP reporter plasmid. Following
303 expression, GFP⁺ cells were isolated by FACS, and then used in antibody blockade
304 experiments, as described above. The results indicated that tetraspanin antibodies blocked
305 MHV infection into normal DBT cells (Fig. 1A and 4A), but not into DBT cells expressing
306 TMPRSS2 (Fig. 4A). Of note, 10⁶ cells transfected with 0.004 µg of TMPRSS2 plasmid
307 contained TMPRSS2 protein levels that were far below our western blot and

308 immunofluorescent assay detection limits, making it clear that even small amounts of
309 priming proteases nullify the antiviral effects of tetraspanin antibodies (Fig. 4A).

310 In similar experiments, PR8 and its priming protease HAT were evaluated in entry
311 assays. Here, 293 β 5 cells were transfected with graded doses of HAT-encoding plasmids,
312 and then infected with PR8, either in the absence or presence of tetraspanin antibodies.
313 The results indicated that HAT bypassed the antibody blockades in a dose-dependent
314 manner (Fig. 4B). Furthermore, trypsin pre-treated viruses also bypassed the antibody
315 blockades (Fig. 4B, rightmost columns). Therefore, the hypothesis that proteases mitigate
316 the antiviral activities of tetraspanin antibodies applies to TMPRSS2, HAT and trypsin
317 proteases, and to MHV and PR8 viruses.

318 ***CD9 knockdown inhibits MERS pp transductions.*** Antibodies binding to CD9,
319 CD81 and CD63 inhibited CoV (MHV) and IAV (PR8) entry (Fig. 1). Amongst these three,
320 CD9 stood out as a candidate for further evaluation, in part because of reports that sperm-
321 egg fusion requires CD9 (41) and HIV -induced fusion requires endogenous CD9 levels
322 (42). Therefore, we evaluated how varying CD9 levels might affect susceptibility to the
323 VSV-based MERS pp transductions. We produced 293 β 5 cells stably expressing hDPP4 and
324 a shRNA against CD9. WB confirmed that these cells expressed hDPP4, but expressed only
325 9% of the CD9 in control cells (Fig. 5A). Notably, the reduced CD9 did not affect any change
326 in the levels of DPP4, unlike that observed by Okamoto et al. (43). In comparison with the
327 vector control and scrambled shRNA control cells, the CD9 knockdown (KD) cells were
328 77% less susceptible to MERS pp transduction. Overexpression of CD9 restored
329 transduction susceptibility to the CD9 KD cells (Fig. 5A). The under- and over-expression of

330 CD9 had no effects on VSV G- mediated transductions (data not shown), indicating a MERS
331 S – specific effect of the CD9 knockdown. All of these results demonstrated that CD9
332 supports MERS at the level of S protein – mediated virus entry.

333 ***Proteases render CD9-knockdown cells susceptible to MERS pp transductions.***

334 To determine whether CD9 knockdown inhibits MERS pp entry at the proteolytic priming
335 stage of entry, we forced protease overexpression by introducing graded doses of
336 TMPRSS2-encoding plasmids, then transduced cells with MERS pp and quantified
337 transduction levels with Fluc measurements. The results of these experiments indicated
338 that excess TMPRSS2 restored transduction sensitivity to CD9-knockdown cells, up to the
339 levels of the CD9-replete cells (Fig. 5B). Specifically, 0.3 μ g TMPRSS2 plasmid / 10^6 cells
340 increased MERS pp transductions by 4 (+/-1) – fold in CD9-positive cells, and 11 (+/-3) –
341 fold in CD9 KD cells (Fig. 5B). These CD9-specific differences were statistically significant
342 ($p < 0.0001$). Thus the impediments to virus entry brought about by CD9 knockdown were
343 overcome by excess proteases.

344 ***TEMs contain CoV receptors and priming proteases.*** Our findings fit with the
345 hypothesis that infecting viruses encounter cell receptors and priming proteases at TEM
346 locations. Antibody binding to TEMs, or omission of particular tetraspanins, interferes with
347 these encounters, reducing infection. We used a biochemical approach to determine
348 whether cell receptors and priming proteases are indeed within TEMs. Surface-
349 biotinylated 293 β 5 cells were lysed in buffers containing CHAPS, a zwitterionic detergent
350 that emulsifies cell membranes without disrupting primary or secondary TEM interactions
351 (44). After sucrose density gradient fractionation, CHAPS-soluble proteins remained near

352 the bottom of sucrose gradients, designated as the high-density (HD) regions, while CHAPS-
353 insoluble protein-lipid complexes floated to the top, low-density (LD) regions. Dot-blotting
354 revealed that ~ 20% of biotinylated (plasma membrane) proteins were in the LD region
355 (Fig. 6A, upper left). Streptavidin pulldowns of the isolated HD and LD fractions revealed
356 that all of the detectable cell-surface CD9, CD63, and CD81 were present in the LD material
357 (Fig. 6A, lower left), indicating that the LD fraction includes the TEMs. Notably, cells lysed
358 by Triton-X 100 (TX-100), a detergent known to solubilize TEMs, also generated an LD
359 fraction that comprised ~20% of plasma membrane proteins (Fig. 6A, upper right), but was
360 devoid of any cell-surface tetraspanins (Fig. 6A, lower right). Thus we designated the
361 CHAPS LD subcellular fractions as “TEMs” and the TX-100 LD fractions as “lipid rafts”.

362 To determine whether CoV receptors and priming proteases partition into TEMs, it
363 was necessary that 293β5 cells were first transfected to overexpress ACE2, APN, CEACAM
364 (the receptor for MHV (45)), or DPP4. The transfected cells were then lysed in CHAPS, and
365 TEMs isolated by two sequential cycles of floatation on sucrose gradients. Western
366 immunoblotting revealed that ~ 90% of ACE2, APN, and CEACAM and ~ 50% of the DPP4,
367 were partitioned into TEM fractions (Fig. 6B). Cells overexpressing the virus-priming
368 proteases TMPRSS2 and HAT were similarly fractionated, and roughly 50% of these
369 proteases were found in the TEM fractions (Fig. 6B). Mature TMPRSS2 and HAT exist as
370 linked cleavage products, and some of the TMPRSS2 and HAT that was not found in TEM
371 (LD) fractions may come from shedding of the FLAG-tagged TMPR ectodomain fragments
372 into soluble (HD) material. An uncleavable TMPRSS2_{S441A} mutant more prominently
373 partitioned into the TEM (LD) fractions. This uncleaved integral-membrane TMPRSS2_{S441A}
374 zymogen may more accurately represent the predominant TEM localization of TMPRs.

375 Some β -actin (<10%) partitioned with TEMs, consistent with known TEM – cytoskeleton
376 interactions (46). Calnexin, a transmembrane protein abundant in the endoplasmic
377 reticulum (47), was excluded from the TEMs, indicating complete cell solubilization by
378 CHAPS detergent. As the TEM fractions contained only ~ 20% of the total plasma
379 membrane proteins, these results indicated that the CoV receptors and priming proteases
380 were at least 5- to 50-fold more abundant in TEMs than elsewhere on cell surfaces. While
381 this is significant microdomain localization, we speculate that these results may be
382 underestimating the extent of receptors and proteases naturally within TEMs, as there are
383 upper limits to accommodating overexpressed receptors and proteases in the TEMs.

384 TEM localization of one CoV receptor (DPP4) and one priming protease (TMPRSS2)
385 was validated by immunofluorescence microscopy. DPP4 and TMPRSS2 were both found
386 near or within CD81-enriched cell-surface puncta (Fig. 7). Similar partitioning of CD81
387 with a catalytically-inactive mutant TMPRSS2_{S441A} was also observed (Fig. 7), indicating
388 that enzymatic activity has no effect on subcellular localization. Thus there are
389 recognizable proportions of CoV receptors and priming proteases residing within TEMs.

390 ***TEMs prime coronaviruses and influenza A viruses for entry.*** To determine
391 whether the isolated TEMs have virus-priming activities, we mixed them with MERS pps,
392 inoculated the mixtures onto susceptible target cells and then measured transduction
393 efficiencies. To ensure that the transduction measurements reflected proteolytic priming
394 by the TEMs, and not by endogenous target cell proteases, we suppressed target 293 β 5-cell
395 priming proteases with leupeptin, a broad-spectrum protease inhibitor. Leupeptin-treated
396 293 β 5 cells were profoundly resistant to MERS pp transduction (Fig. 8A; top), indicative of

397 requirements for the host proteases. However, MERS pp that were exposed to TEM
398 fractions transduced the leupeptin-treated cells (Fig. 8A, top), indicating priming. Of note,
399 the bypass of leupeptin was pronounced when MERS pp were exposed to trypsin, or to
400 TEMs containing overexpressed TMPRSS2, but did not reach the levels observed in the
401 absence of leupeptin. In addition, substantial bypass of leupeptin was not achieved by
402 CHAPS HD fractions (data not shown), even though the HD fractions included all soluble
403 proteins as well as ~ 80% of the plasma membrane proteins (Fig. 6A). These findings
404 indicated that MERS entry-priming activities were greatly concentrated in the TEMs.

405 MERS pp that had been exposed to TEMs were also evaluated to assess the extents
406 of S protein cleavage. Western immunoblots indicated that the TEMs effected cleavage of S
407 proteins, generating proteolytic patterns that were indistinguishable from those generated
408 by trypsin (Fig. 8A; bottom). The apparent molecular weights of the N-linked glycoprotein
409 products were consistent with cleavages at three multibasic sites, one at 626-629 (RQQR)
410 to create the minor 130 kDa fragment, one at 884-887 (RSAR) to create the major 70 kDa
411 fragment, and one at 1110-1113 (QSKR) to create the minor 40 kDa fragment. The major
412 70 kDa fragment has molecular weight equivalent to the previously documented S2' (1).

413 Analogous experiments were completed with IAV PR8 viruses. In these assays,
414 however, inactivation of host proteases by leupeptin was not required, as PR8 did not
415 respond to endogenous levels of 293-cell proteases. The results of these experiments
416 demonstrated that TEM fractions activated PR8 infectivities, nearly as much as TEMs with
417 overexpressed HAT (Fig. 8B, top). The fact that the TEMs were isolated from IAV-resistant
418 293β5 cells, yet were capable of priming IAV for infection, are potentially explained by the
419 significant concentration of cell proteases achieved through TEM isolation.

420 As with the MERS S on viral pps, PR8-associated HA proteins were analyzed for
421 cleavage status by western immunoblotting. Here, the TEMs effected cleavage of HA0 into
422 HA1, irrespective of whether HAT was overexpressed and equal to that achieved by trypsin
423 (Fig. 8B; bottom). Thus the TEM fractions harvested from 293 cells have proteases that
424 cleave and prime both MERS-CoV S and PR8 IAV HA proteins.

425 **DISCUSSION**

426 We evaluated TEMs for host-cell entry factors and determined that they contain
427 both CoV receptors and transmembrane serine proteases (TMPRs), and were capable of
428 cleaving and priming CoV and IAV fusion proteins. We did not determine whether IAV
429 sialic acid receptors are concentrated in TEMs, but there is evidence of sialylated proteins
430 associating with tetraspanins (21, 48, 49). The findings suggested that, in natural
431 infections, the CoVs and LP IAVs encounter TEMs during their cell entry, and in doing so
432 become proteolytically primed. This suggestion was consistent with virus entry blockades
433 by tetraspanin antibodies, and with reduced virus entry upon depletion of the tetraspanin
434 CD9. From these results, we have come to the view that TEMs are platforms for several
435 CoV and for LP IAV proteolytic priming events.

436 Previous investigators have hypothesized that TEMs are more flexible or curved
437 than other membrane regions and therefore provide a platform that is more favorable for
438 membrane melding. For example, in mouse oocytes, TEMs facilitate cell membrane
439 wrinkling, which hypothetically lowers the kinetic barrier to fusion with sperm-cell
440 membranes (41). However, in the virus-cell membrane fusions that we have evaluated, it
441 seems that TEMs do not facilitate the membrane fusions *per se*, but rather facilitate virus

442 proteolytic priming. This claim arises in part because tetraspanin antibodies blocked MHV
443 and PR8 infections (Fig. 1) but not when transmembrane protease concentrations were
444 elevated (Fig. 4). With respect to the mechanisms by which tetraspanin antibodies block
445 virus entry, one possibility is that the bivalent antibodies hold tetraspanins together,
446 rigidifying TEMs and impeding membrane protein movements. Reduced diffusion of virus-
447 receptor complexes might therefore increase the time required for viruses to encounter
448 proteases. Increasing protease concentrations might ease this supposed requirement for
449 lateral mobility of receptor-bound viruses. Another possibility is that transmembrane
450 protease activities depend on precise embedment into TEMs, with tetraspanin antibodies
451 interfering with this hypothetical positioning. This notion has some support from our
452 finding that CD9 depletions reduced MERS pp transductions at the level of MERS S protein
453 proteolytic priming.

454 Even with a restricted focus on TEMs as virus entry portals, it remains challenging
455 to identify which cellular proteases are utilized for CoV S and IAV HA priming. For LP IAV,
456 the relevant priming proteases are known to include TMPRSS2 (14) and HAT (15). The
457 CoVs appear to be less restricted in their protease requirements, and members may utilize
458 many or all of the ~19 TMPRs (5), as well as the ~25 membrane metalloproteinases (50).
459 TMPRSS2, however, stands out as a key CoV-priming protease (3, 6-9, 51). Perhaps
460 TMPRSS2 is more promiscuous with substrates than the other TTSPs, although any
461 evidence for this is lacking. Alternatively, TMPRSS2 may act as a “master” protease that
462 cleaves nearby zymogens, activating them in proteolytic cascades (52). Other TMPRSS2-
463 activated proteases may then cleave CoV S proteins. In addition, some CoVs may bypass
464 TEM-associated proteases, undergoing cleavage-priming after endocytosis. A key example

465 here is with MHV-2, which utilizes endosomal cathepsins to prime S proteins for entry (53).
466 There is no evidence that cathepsins are localized to TEMs. Thus the requirements for
467 TEM-associated cleavage events may depend on the CoV strain, and on the particular
468 combinations of virus-priming proteases in target cells. Analyses of clinical CoV isolates for
469 their entry into cells reflecting *in vivo* infection environments may be necessary to assess
470 the importance TEM-associated S proteolysis in natural infection and disease, for example,
471 by using transgenic mice lacking TMPRSS2^{-/-} (54) and HAT^{-/-} (55).

472 The human CoVs use the transmembrane ectopeptidases ACE2 (38), APN (36), and
473 DPP4 (37) as host cell receptors. These receptors do not share any obvious structural
474 similarities, and while they do share ectopeptidase activities, these enzymatic functions are
475 dispensable for virus entry (36-38). Localization in TEMs, therefore, may be a shared
476 feature that is relevant to the selection of these ectopeptidases as CoV receptors. One
477 possibility is that the CoVs evolved to use TEM-associated receptors so that, once bound to
478 cells, the viruses are poised for cleavage by TEM-resident proteases. It is, however, also
479 possible that the viruses, adapted to TEM-associated receptors for yet unknown reasons,
480 evolved to utilize nearby proteases for cleavage and priming. This evolution of viruses for
481 particular receptors and proteases, when viewed in a dynamic context, posits that receptor
482 binding elicits structural changes in viral spikes that transiently expose proteolytic
483 substrates. Without proteases nearby, uncleaved intermediate S conformers might
484 continue through unproductive folding pathways that are incompatible with virus entry.
485 Conceivably, the proteolytic TEM environment is the preferred location for receptor-
486 induced conformational changes of S proteins, rapid proteolytic cleavage of the

487 intermediate S conformations, and possibly the subsequent refolding to postfusion forms,
488 in spatial and temporal patterns that foster efficient virus entry.

489 Distinctions between TEMs and lipid rafts are noteworthy. TEMs are operationally
490 distinguished from classical lipid rafts by their insolubility in zwitterionic detergents such
491 as CHAPS and Brij98 (56), and by their complete disruption by nonionic detergents such as
492 TX100 ((44) and Fig. 6). However, both TEM and lipid rafts are enriched in cholesterol,
493 sphingolipids, and GPI-linked surface proteins (16, 57-59), and cholesterol chelators such
494 as cyclodextrins will disrupt both TEM and lipid raft architectures (60, 61). These common
495 features of TEMs and lipid rafts can make it difficult to determine which microdomain
496 serves as a virus entry site. For example, cholesterol depletion decreases CoV-cell entry,
497 and it is re-supplementation restores entry (27, 62). Similar results were obtained in
498 studies of IAV entry (63). The TEM-disrupting effects of cyclodextrins, in conjunction with
499 our observations of TEM-associated virus receptors and virus-priming proteases, raise the
500 possibility that cholesterol depletions block virus entry by separating receptors from
501 priming proteases in TEMs. This suggestion can be addressed by determining whether pre-
502 primed viruses are resistant to cholesterol starvation. Revisiting previous studies with
503 greater attention paid to distinguishing TEMs and lipid rafts may yield additional insights
504 into the subcellular locations of CoV and IAV cell entry.

505 Determining the subcellular location of virus priming events has implications for
506 development of antiviral drugs, including antiviral proteases. Currently, broad spectrum
507 protease inhibitors can be used to prevent viral infection and spread both *in vitro* (64) and
508 *in vivo* (65), but these treatments are not approved for human use and there is little data on

509 their efficacy or side effects. By targeting protease inhibitors to TEMs, one might increase
510 inhibitor potencies, and also elicit antiviral activity without causing undesired reductions
511 of total lung proteolytic activity. To achieve this targeting, inhibitors might be conjugated
512 to TEM-binding motifs, such as those found on the hepatitis C virus E2 protein (66), or to
513 components of TEMs such as cholesterol. With respect to cholesterol, it has already been
514 demonstrated that inhibitors of virus entry are potentiated by linkage to cholesterol
515 moieties (67). These cholesterol-conjugated inhibitors are helical peptides that target
516 transient folding intermediates of viral glycoproteins, preventing their ability to catalyze
517 membrane fusion and thus blocking virus entry. We suggest, at least for the CoVs, that
518 these intermediates are formed subsequent to proteolytic priming in TEMs. Helical
519 peptides targeting these CoV intermediates are well-described (68, 69), and targeting these
520 peptides to the TEM locus of priming may increase their antiviral efficacies.

521 **ACKNOWLEDGMENTS**

522 The authors thank Drs. Lijun Rong, Fang Li, and Michael Farzan for plasmid DNAs, Dr.
523 Michael Whitt for recombinant VSVs, Dr. Peter Palese for recombinant IAV, and Dr. Balaji
524 Manicassamy for anti-IAV antibodies. We especially thank Dr. Edward Campbell for expert
525 support with immunofluorescent microscopy experiments and Dr. Stanley Perlman for
526 manuscript comments. This work was supported by NIH grants R56AI092128 and
527 P01AI060699.

528 **FIGURE LEGENDS**

529 **Figure 1. Effect of tetraspanin antibodies on MHV and IAV infection. (A)** DBT cells
530 were treated with monoclonal antibodies to CD9, CD63, CD81, or an equimolar mixture of

531 the three tetraspanin antibodies (α Tspan). After 30 min at 37°C, cells were infected with
532 recombinant MHV-A59 or MHV-JHM viruses containing a firefly luciferase (Fluc) reporter
533 gene. Following a 2 h entry period, unadsorbed antibody and virus was removed. 8 hpi,
534 infection levels were measured by quantifying Fluc reporter gene products and were
535 normalized to the untreated controls. A VSV-G pp reporter virus was also used. Mouse
536 immunoglobulin G (M-IgG) and monoclonal antibody against transferrin receptor (TfR)
537 were used as controls for antibody subtype and irrelevant cell binding, respectively.
538 Results are representative of three independent experiments. * $p < 0.05$ when compared to
539 “No Ab”. **(B)** Cells transfected with an empty vector (EV), 0.1 μ g TMPRSS2/10⁶ cells, or
540 increasing amounts of HAT plasmid were infected with a PR8 influenza virus containing a
541 *Gaussia* luciferase (Gluc) reporter gene. Unadsorbed virus was removed after a 2 h entry
542 period. 8 hpi, media was removed from cells and analyzed for Gluc expression. **(C)** 293 β 5
543 cells transfected with 0.001 μ g HAT/10⁶ cells were treated with antibodies as described in
544 (A). This experiment also included a non-specific Mouse IgG control antibody (M Ig).
545 Media was collected and analyzed for secreted Gluc 8 hpi. * $p < 0.05$ when compared to “No
546 Ab”.

547 **Figure 2. Effect of tetraspanin antibodies on CoV pp cell entry.** **(A)** 293 β 5 cells
548 overexpressing appropriate receptors (APN for 229E, DPP4 for MERS, ACE2 for SARS) were
549 treated with monoclonal antibodies to CD9, CD63, CD81, or an equimolar mixture of the
550 three tetraspanin antibodies (α Tspan). After 30 min at 37°C, the indicated VSV pps bearing
551 the spike proteins from 229E (black), MERS (gray), or SARS (hatched) were inoculated for
552 2h at 37°C, and unadsorbed virus and antibody were then removed from cells.
553 Transduction levels were measured by quantifying Fluc reporter gene products and were

554 normalized to the untreated controls. Mouse IgG (M Ig) and a monoclonal antibody against
555 transferrin receptor (TfR) were used as controls for antibody subtype and irrelevant cell
556 binding, respectively. Results are representative of three independent experiments.
557 * $p < 0.05$ when compared to the “No Ab” controls. **(B)** 293 β 5 cells were incubated without
558 antibodies (-), with control anti-transferrin receptor antibodies (α TfR), or with a mixture of
559 anti-tetraspanin antibodies (α Tspan) for 30 min periods immediately before (-30) or after
560 (+30) a 60 min VSV-MERS S pp inoculation period. Transduction levels were measured by
561 quantifying luciferase accumulations and were normalized to the controls in which
562 antibodies were not applied. * $p < 0.05$ when compared to “No Ab”.

563 **Figure 3. Immunofluorescent analysis of pp binding to cells in the presence of**
564 **tetraspanin antibodies. (A)** Flow cytometric analysis of the binding efficiencies of the
565 antibodies used in tetraspanin blockade experiments. 293 β 5 cells were incubated without
566 antibodies (black) or with the indicated antibodies. Following a 30 minute incubation, cells
567 were washed and incubated with an anti-mouse AlexaFluor-488 (AF488) secondary
568 antibody. Flow cytometry was performed to detect levels of AF488 intensity of treated
569 cells. **(B)** 293 β 5 cells overexpressing DPP4 (+DPP4) or an empty vector (-DPP4) were
570 incubated with HIV-mCherry MERS pp for 1 h at 4°C. Following incubation, cells were
571 washed of unbound virus and analyzed by flow cytometry to detect levels of mCherry. The
572 percentage of mCherry-positive cells is indicated above the gate (left panel). +DPP4 cells
573 were treated with α Tspan antibodies. After 30 min at 37°C, HIV-mCherry-MERS pps were
574 inoculated for 120 min at 4°C. Following washing of unadsorbed virus and antibody, flow
575 cytometry was performed to detect bound HIV-based pps (right panel). **(C)** HIV-mCherry
576 pps without protruding glycoproteins (Bald) or with VSV G, IAV HA, or MERS S, were mixed

577 with anti-CD81 antibodies and inoculated onto +DPP4 cells for 30 min at 4°C. After a 10-
578 min, 37°C patching period, cells were fixed and analyzed by confocal microscopy to
579 determine the location of the pps (red) and CD81 (green). Co-localization of CD81 and HIV-
580 positive puncta were quantified using Imaris software. Data were plotted as percent of HIV-
581 – based pps that were localized to CD81.

582 **Figure 4. Effect of proteases on tetraspanin antibody-blocked infections. (A)** DBT
583 cells were transfected with increasing amounts of Tmprss2 plasmid and a small amount of
584 GFP reporter. Following isolation of transfected cells by FACS, cells were treated with
585 either a mixture of tetraspanin antibodies (+ α Tspan) or media (- α Tspan). After 30 min,
586 cells were infected with MHV-JHM. 2 hpi, cells were washed to removed unadsorbed virus
587 and antibody. 8 hpi cells were lysed and analyzed for Fluc reporter expression. Data were
588 graphed as Fluc RLU per cell. **(B)** 293 β 5 cells were transfected with the indicated amounts
589 of HAT before being exposed to the same Tspan antibody blockade described in (A). Cells
590 were then infected with PR8-Gluc for 2 h, washed, and secreted Gluc was measured 8 hpi.
591 PR8 viruses pre-treated with trypsin (+Trypsin) were also infected onto cells transfected
592 with 0.001 μ g HAT/10⁶ cells (rightmost columns).

593 **Figure 5. Effect of CD9 knockdown on MERS pp entry. (A)** 293 β 5 cells stably
594 expressing DPP4 and either an empty shRNA vector (EV), a scrambled shRNA, or an shRNA
595 specific for CD9 were transfected with an empty vector (-CD9 cDNA) or a vector containing
596 CD9 cDNA (+CD9 cDNA). These cells were transduced with MERS pp and transduction
597 levels measured by Fluc reporter gene expression. Cell lysates were analyzed by western
598 blot for CD9 and β -actin (below graph). **(B)** Cells stably expressing EV, a scrambled shRNA,

599 or a CD9 shRNA were transfected with increasing amounts of TMPRSS2 before
600 transduction with MERS pp. Transduction levels were measured by Fluc reporter gene
601 expression.

602 **Figure 6. Isolation and analysis of TEM fractions. (A)** 293 β 5 cells were surface-
603 biotinylated before lysis with CHAPS or TX-100. Following differential centrifugation, 10
604 fractions were collected from each tube and analyzed for total-cell surface, biotinylated
605 proteins (top). Following collection of HD and LD fraction, streptavidin pulldowns were
606 performed and each fraction was analyzed for cell surface CD9, CD63, and CD81 (bottom).
607 **(B)** 293 β 5 cells overexpressing epitope-tagged CoV receptors ACE2, APN, CEACAM, and
608 DPP4, or Flag-tagged TTSPs TMPRSS2, TMPRSS2-S441A or HAT. Transfected cells were
609 subjected to CHAPS lysis and density gradient centrifugation, as described in (A). Western
610 blot was used to determine separation of the indicated proteins into HD and LD fractions.
611 β -actin and calnexin were used as controls for complete cell lysis and proteins not present
612 in CHAPS LDs.

613 **Figure 7. Localization of MERS-CoV entry factors DPP4 and TMPRSS2 in relation to**
614 **tetraspanin CD81.** 293 β 5 cells were transfected with plasmids encoding the indicated
615 Flag-tagged proteins. 24 h later, live cells were co-incubated with anti-Flag and anti-CD81
616 antibodies, with a 10-min incubation at 37C to induce patching. Fluorescent secondary
617 antibodies were applied to mark the positions of Flag-tagged proteins and CD81, and
618 Hoescht 33258 (blue) mark the positions of cell nuclei. Images show 0.5-micron thick
619 confocal slices through the middle section of cells.

620 **Figure 8. CoV priming activity of TEMs. (A)** MERS pps were used to transduce 293β5
621 cells treated with leupeptin or a media control. Prior to transduction, MERS pps were
622 treated with trypsin, TEMs isolated from untransfected cells, or TEMs isolated from
623 TMPRSS2 overexpressing cells. Transduction levels were measured by luciferase reporter
624 gene expression (top). These MERS pps were also concentrated and analyzed by western
625 blot with an antibody to detect a C-terminal C9 tag on the MERS spike (bottom) **(B)** 293β5
626 cells were infected with PR8 that was treated with trypsin, TEMs isolated from
627 untransfected cells, or TEMs from HAT overexpressing cells. Infection was measured by
628 Gluc expression (top). Viruses were concentrated and analyzed by western blot (bottom).
629 *p<0.05 when compared to (-) incubation.

630 REFERENCES

- 631 1. **Millet JK, Whittaker GR.** 2014. Host cell entry of Middle East respiratory syndrome
632 coronavirus after two-step, furin-mediated activation of the spike protein. Proceedings of
633 the National Academy of Sciences of the United States of America **111**:15214-15219.
- 634 2. **Kido H, Yokogoshi Y, Sakai K, Tashiro M, Kishino Y, Fukutomi A, Katunuma N.** 1992.
635 Isolation and characterization of a novel trypsin-like protease found in rat bronchiolar
636 epithelial Clara cells. A possible activator of the viral fusion glycoprotein. The Journal of
637 biological chemistry **267**:13573-13579.
- 638 3. **Bertram S, Heurich A, Lavender H, Gierer S, Danisch S, Perin P, Lucas JM, Nelson PS,**
639 **Pohlmann S, Soilleux EJ.** 2012. Influenza and SARS-coronavirus activating proteases
640 TMPRSS2 and HAT are expressed at multiple sites in human respiratory and
641 gastrointestinal tracts. PloS one **7**:e35876.
- 642 4. **Zhirnov OP, Klenk HD, Wright PF.** 2011. Aprotinin and similar protease inhibitors as
643 drugs against influenza. Antiviral research **92**:27-36.
- 644 5. **Bugge TH, Antalis TM, Wu Q.** 2009. Type II Transmembrane Serine Proteases. Journal of
645 Biological Chemistry **284**:23177-23181.
- 646 6. **Glowacka I, Bertram S, Muller MA, Allen P, Soilleux E, Pfefferle S, Steffen I, Tsegaye TS,**
647 **He Y, Gnirss K, Niemeyer D, Schneider H, Drosten C, Pohlmann S.** 2011. Evidence that
648 TMPRSS2 activates the severe acute respiratory syndrome coronavirus spike protein for
649 membrane fusion and reduces viral control by the humoral immune response. Journal of
650 virology **85**:4122-4134.
- 651 7. **Shulla A, Heald-Sargent T, Subramanya G, Zhao J, Perlman S, Gallagher T.** 2011. A
652 transmembrane serine protease is linked to the severe acute respiratory syndrome
653 coronavirus receptor and activates virus entry. Journal of virology **85**:873-882.

- 654 8. **Shirato K, Kawase M, Matsuyama S.** 2013. Middle East Respiratory Syndrome Coronavirus
655 Infection Mediated by the Transmembrane Serine Protease TMPRSS2. *Journal of virology*
656 **87:12552-12561.**
- 657 9. **Gierer S, Bertram S, Kaup F, Wrensch F, Heurich A, Kramer-Kuhl A, Welsch K, Winkler**
658 **M, Meyer B, Drosten C, Dittmer U, von Hahn T, Simmons G, Hofmann H, Pohlmann S.**
659 2013. The spike protein of the emerging betacoronavirus EMC uses a novel coronavirus
660 receptor for entry, can be activated by TMPRSS2, and is targeted by neutralizing antibodies.
661 *Journal of virology* **87:5502-5511.**
- 662 10. **Bertram S, Dijkman R, Habjan M, Heurich A, Gierer S, Glowacka I, Welsch K, Winkler**
663 **M, Schneider H, Hofmann-Winkler H, Thiel V, Pohlmann S.** 2013. TMPRSS2 activates the
664 human coronavirus 229E for cathepsin-independent host cell entry and is expressed in viral
665 target cells in the respiratory epithelium. *Journal of virology* **87:6150-6160.**
- 666 11. **Kawase M, Shirato K, Matsuyama S, Taguchi F.** 2009. Protease-mediated entry via the
667 endosome of human coronavirus 229E. *Journal of virology* **83:712-721.**
- 668 12. **Simmons G, Gosalia DN, Rennekamp AJ, Reeves JD, Diamond SL, Bates P.** 2005.
669 Inhibitors of cathepsin L prevent severe acute respiratory syndrome coronavirus entry.
670 *Proceedings of the National Academy of Sciences of the United States of America*
671 **102:11876-11881.**
- 672 13. **Bottcher E, Matrosovich T, Beyerle M, Klenk HD, Garten W, Matrosovich M.** 2006.
673 Proteolytic activation of influenza viruses by serine proteases TMPRSS2 and HAT from
674 human airway epithelium. *Journal of virology* **80:9896-9898.**
- 675 14. **Hatesuer B, Bertram S, Mehnert N, Bahgat MM, Nelson PS, Pohlman S, Schughart K.**
676 2013. Tmprss2 is essential for influenza H1N1 virus pathogenesis in mice. *PLoS pathogens*
677 **9:e1003774.**
- 678 15. **Bottcher-Friebertshauser E, Freuer C, Sielaff F, Schmidt S, Eickmann M, Uhlenborff J,**
679 **Steinmetzer T, Klenk HD, Garten W.** 2010. Cleavage of influenza virus hemagglutinin by
680 airway proteases TMPRSS2 and HAT differs in subcellular localization and susceptibility to
681 protease inhibitors. *Journal of virology* **84:5605-5614.**
- 682 16. **Charrin S, le Naour F, Silvie O, Milhiet PE, Boucheix C, Rubinstein E.** 2009. Lateral
683 organization of membrane proteins: tetraspanins spin their web. *The Biochemical journal*
684 **420:133-154.**
- 685 17. **Yanez-Mo M, Barreiro O, Gordon-Alonso M, Sala-Valdes M, Sanchez-Madrid F.** 2009.
686 Tetraspanin-enriched microdomains: a functional unit in cell plasma membranes. *Trends in*
687 *cell biology* **19:434-446.**
- 688 18. **van Spriel AB, Figdor CG.** 2010. The role of tetraspanins in the pathogenesis of infectious
689 diseases. *Microbes and infection / Institut Pasteur* **12:106-112.**
- 690 19. **Le Naour F, Andre M, Boucheix C, Rubinstein E.** 2006. Membrane microdomains and
691 proteomics: lessons from tetraspanin microdomains and comparison with lipid rafts.
692 *Proteomics* **6:6447-6454.**
- 693 20. **Rana S, Claas C, Kretz CC, Nazarenko I, Zoeller M.** 2011. Activation-induced
694 internalization differs for the tetraspanins CD9 and Tspan8: Impact on tumor cell motility.
695 *The international journal of biochemistry & cell biology* **43:106-119.**
- 696 21. **Ono M, Hakomori S.** 2003. Glycosylation defining cancer cell motility and invasiveness.
697 *Glycoconj J* **20:71-78.**
- 698 22. **Andre M, Le Caer JP, Greco C, Planchon S, El Nemer W, Boucheix C, Rubinstein E,**
699 **Chamot-Rooke J, Le Naour F.** 2006. Proteomic analysis of the tetraspanin web using LC-
700 ESI-MS/MS and MALDI-FTICR-MS. *Proteomics* **6:1437-1449.**
- 701 23. **He J, Sun E, Bujny MV, Kim D, Davidson MW, Zhuang X.** 2013. Dual function of CD81 in
702 influenza virus uncoating and budding. *PLoS pathogens* **9:e1003701.**

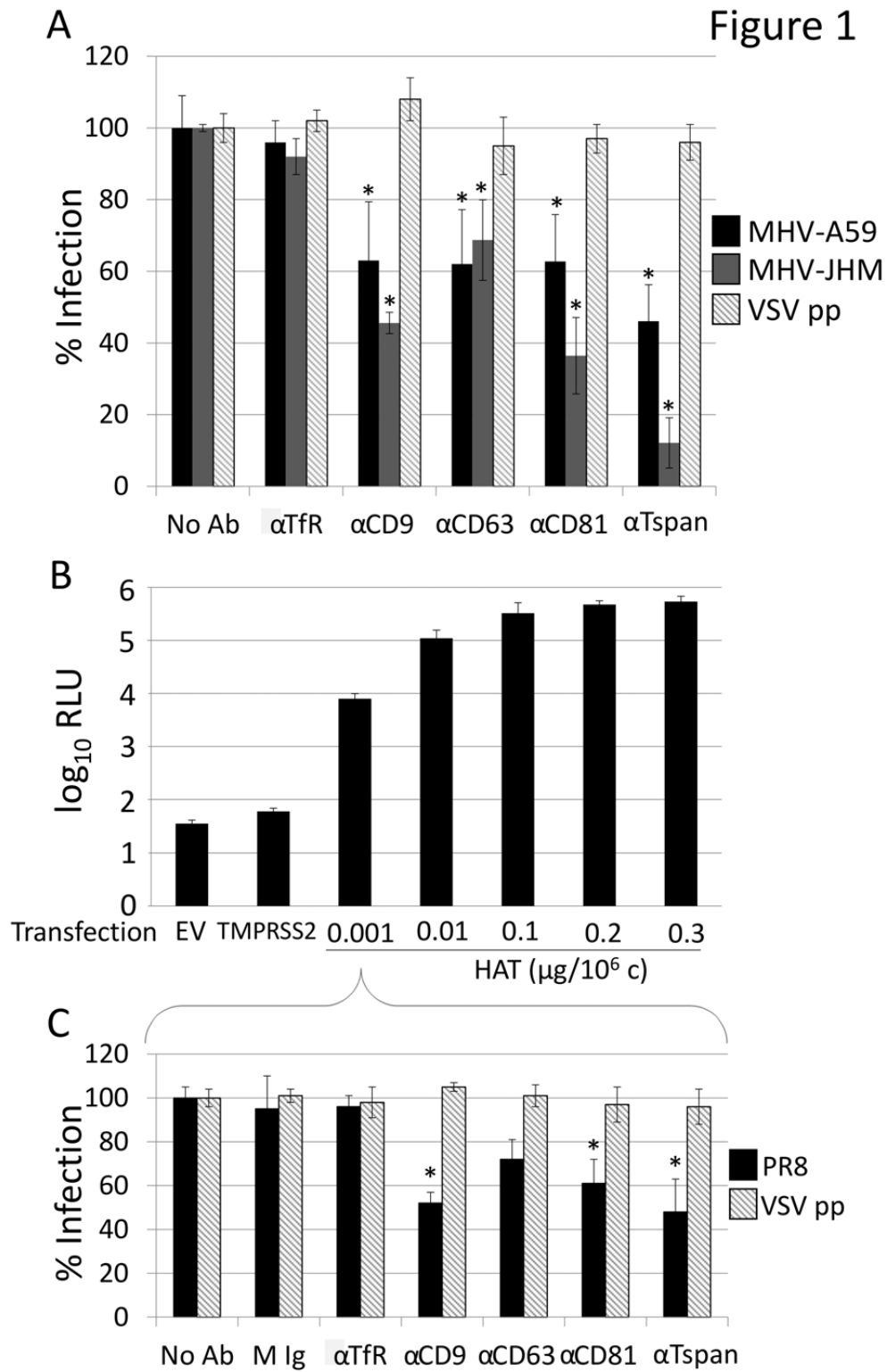
- 703 24. **Konig R, Stertz S, Zhou Y, Inoue A, Hoffmann HH, Bhattacharyya S, Alamares JG,**
704 **Tscherne DM, Ortigoza MB, Liang Y, Gao Q, Andrews SE, Bandyopadhyay S, De Jesus P,**
705 **Tu BP, Pache L, Shih C, Orth A, Bonamy G, Miraglia L, Ideker T, Garcia-Sastre A, Young**
706 **JA, Palese P, Shaw ML, Chanda SK.** 2010. Human host factors required for influenza virus
707 replication. *Nature* **463**:813-817.
- 708 25. **Nguyen EK, Nemerow GR, Smith JG.** 2010. Direct evidence from single-cell analysis that
709 human {alpha}-defensins block adenovirus uncoating to neutralize infection. *Journal of*
710 *virology* **84**:4041-4049.
- 711 26. **Rumschlag-Booms E, Guo Y, Wang J, Caffrey M, Rong L.** 2009. Comparative analysis
712 between a low pathogenic and a high pathogenic influenza H5 hemagglutinin in cell entry.
713 *Virology journal* **6**:76.
- 714 27. **Thorp EB, Gallagher TM.** 2004. Requirements for CEACAMs and cholesterol during murine
715 coronavirus cell entry. *Journal of virology* **78**:2682-2692.
- 716 28. **Campbell EM, Perez O, Melar M, Hope TJ.** 2007. Labeling HIV-1 virions with two
717 fluorescent proteins allows identification of virions that have productively entered the
718 target cell. *Virology* **360**:286-293.
- 719 29. **Heaton NS, Levya-Grado VH, Tan GS, Eggink D, Hai R, Palese P.** 2013. *In vivo*
720 bioluminescent imaging of influenza A virus infection and characterization of novel cross-
721 protective monoclonal antibodies. *Journal of virology* **87**:8272.
- 722 30. **Szretter KJ, Balish AL, Katz JM.** 2006. Influenza: propagation, quantification, and storage.
723 *Current protocols in microbiology* **Chapter 15**:Unit 15G 11.
- 724 31. **Shulla A, Gallagher T.** 2009. Role of spike protein endodomains in regulating coronavirus
725 entry. *The Journal of biological chemistry* **284**:32725-32734.
- 726 32. **Whitt MA.** 2010. Generation of VSV pseudotypes using recombinant DeltaG-VSV for studies
727 on virus entry, identification of entry inhibitors, and immune responses to vaccines. *Journal*
728 *of virological methods* **169**:365-374.
- 729 33. **Barlan A, Zhao J, Sarkar MK, Li K, McCray PB, Jr., Perlman S, Gallagher T.** 2014.
730 Receptor variation and susceptibility to Middle East respiratory syndrome coronavirus
731 infection. *Journal of virology* **88**:4953-4961.
- 732 34. **Bartosch B, Vitelli A, Granier C, Goujon C, Dubuisson J, Pascale S, Scarselli E, Cortese R,**
733 **Nicosia A, Cosset F-L.** 2003. Cell Entry of Hepatitis C Virus Requires a Set of Co-receptors
734 That Include the CD81 Tetraspanin and the SR-B1 Scavenger Receptor. *Journal of Biological*
735 *Chemistry* **278**:41624-41630.
- 736 35. **Scheffer KD, Gawlitza A, Spoden GA, Zhang XA, Lambert C, Berditchevski F, Florin L.**
737 2013. Tetraspanin CD151 mediates papillomavirus type 16 endocytosis. *Journal of virology*
738 **87**:3435-3446.
- 739 36. **Yeager CL, Ashmun RA, Williams RK, Cardellicchio CB, Shapiro LH, Look AT, Holmes**
740 **KV.** 1992. Human aminopeptidase N is a receptor for human coronavirus 229E. *Nature*
741 **357**:420-422.
- 742 37. **Raj VS, Mou H, Smits SL, Dekkers DH, Muller MA, Dijkman R, Muth D, Demmers JA,**
743 **Zaki A, Fouchier RA, Thiel V, Drosten C, Rottier PJ, Osterhaus AD, Bosch BJ, Haagmans**
744 **BL.** 2013. Dipeptidyl peptidase 4 is a functional receptor for the emerging human
745 coronavirus-EMC. *Nature* **495**:251-254.
- 746 38. **Li W, Moore MJ, Vasilieva N, Sui J, Wong SK, Berne MA, Somasundaran M, Sullivan JL,**
747 **Luzuriaga K, Greenough TC, Choe H, Farzan M.** 2003. Angiotensin-converting enzyme 2 is
748 a functional receptor for the SARS coronavirus. *Nature* **426**:450-454.
- 749 39. **Ziyyat A, Rubinstein E, Monier-Gavelle F, Barraud V, Kulski O, Prenant M, Boucheix C,**
750 **Bomsel M, Wolf JP.** 2006. CD9 controls the formation of clusters that contain tetraspanins
751 and the integrin alpha 6 beta 1, which are involved in human and mouse gamete fusion.
752 *Journal of cell science* **119**:416-424.

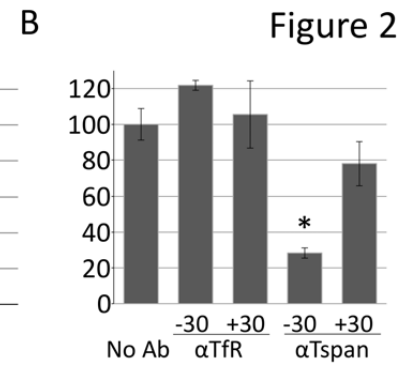
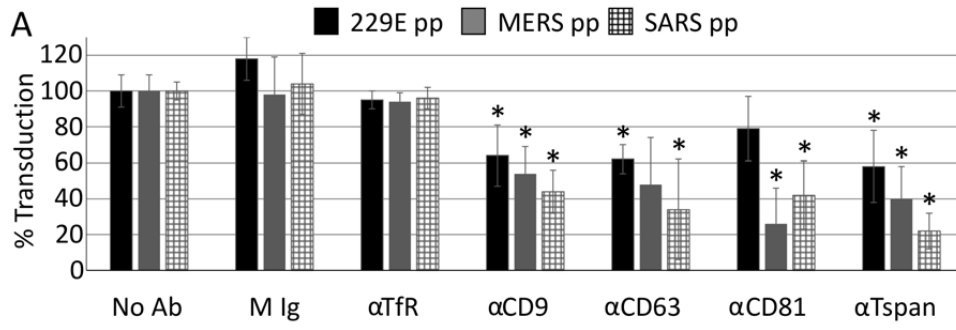
- 753 40. **Matsuyama S, Nagata N, Shirato K, Kawase M, Takeda M, Taguchi F.** 2010. Efficient
754 activation of the severe acute respiratory syndrome coronavirus spike protein by the
755 transmembrane protease TMPRSS2. *Journal of virology* **84**:12658-12664.
- 756 41. **Runge KE, Evans JE, He ZY, Gupta S, McDonald KL, Stahlberg H, Primakoff P, Myles DG.**
757 2007. Oocyte CD9 is enriched on the microvillar membrane and required for normal
758 microvillar shape and distribution. *Developmental biology* **304**:317-325.
- 759 42. **Symeonides M, Lambele M, Roy NH, Thali M.** 2014. Evidence showing that tetraspanins
760 inhibit HIV-1-induced cell-cell fusion at a post-hemifusion stage. *Viruses* **6**:1078-1090.
- 761 43. **Okamoto T, Iwata S, Yamazaki H, Hatano R, Komiya E, Dang NH, Ohnuma K, Morimoto**
762 **C.** 2014. CD9 negatively regulates CD26 expression and inhibits CD26-mediated
763 enhancement of invasive potential of malignant mesothelioma cells. *PLoS one* **9**:e86671.
- 764 44. **Claas C, Stipp CS, Hemler ME.** 2001. Evaluation of prototype transmembrane 4
765 superfamily protein complexes and their relation to lipid rafts. *The Journal of biological*
766 *chemistry* **276**:7974-7984.
- 767 45. **Dveksler GS, Pensiero MN, Cardellicchio CB, Williams RK, Jiang GS, Holmes KV,**
768 **Dieffenbach CW.** 1991. Cloning of the mouse hepatitis virus (MHV) receptor: expression in
769 human and hamster cell lines confers susceptibility to MHV. *Journal of virology* **65**:6881-
770 6891.
- 771 46. **Sala-Valdes M, Ursa A, Charrin S, Rubinstein E, Hemler ME, Sanchez-Madrid F, Yanez-**
772 **Mo M.** 2006. EWI-2 and EWI-F link the tetraspanin web to the actin cytoskeleton through
773 their direct association with ezrin-radixin-moesin proteins. *The Journal of biological*
774 *chemistry* **281**:19665-19675.
- 775 47. **Wada I, Rindress D, Cameron PH, Ou WJ, Doherty JJ, 2nd, Louvard D, Bell AW, Dignard**
776 **D, Thomas DY, Bergeron JJ.** 1991. SSR alpha and associated calnexin are major calcium
777 binding proteins of the endoplasmic reticulum membrane. *The Journal of biological*
778 *chemistry* **266**:19599-19610.
- 779 48. **Cannon KS, Cresswell P.** 2001. Quality control of transmembrane domain assembly in the
780 tetraspanin CD82. *The EMBO journal* **20**:2443-2453.
- 781 49. **Toledo MS, Suzuki E, Handa K, Hakomori S.** 2005. Effect of ganglioside and tetraspanins
782 in microdomains on interaction of integrins with fibroblast growth factor receptor. *The*
783 *Journal of biological chemistry* **280**:16227-16234.
- 784 50. **Bourboulia D, Stetler-Stevenson WG.** 2010. Matrix metalloproteinases (MMPs) and tissue
785 inhibitors of metalloproteinases (TIMPs): Positive and negative regulators in tumor cell
786 adhesion. *Seminars in Cancer Biology* **20**:161-168.
- 787 51. **Heurich A, Hofmann-Winkler H, Gierer S, Liepold T, Jahn O, Pohlmann S.** 2014.
788 TMPRSS2 and ADAM17 Cleave ACE2 Differentially and Only Proteolysis by TMPRSS2
789 Augments Entry Driven by the Severe Acute Respiratory Syndrome Coronavirus Spike
790 Protein. *Journal of virology* **88**:1293-1307.
- 791 52. **Lin B, Ferguson C, White JT, Wang S, Vessella R, True LD, Hood L, Nelson PS.** 1999.
792 Prostate-localized and Androgen-regulated Expression of the Membrane-bound Serine
793 Protease TMPRSS2. *Cancer Research* **59**:4180-4184.
- 794 53. **Qiu Z, Hingley ST, Simmons G, Yu C, Das Sarma J, Bates P, Weiss SR.** 2006. Endosomal
795 proteolysis by cathepsins is necessary for murine coronavirus mouse hepatitis virus type 2
796 spike-mediated entry. *Journal of virology* **80**:5768-5776.
- 797 54. **Kim TS, Heinlein C, Hackman RC, Nelson PS.** 2006. Phenotypic Analysis of Mice Lacking
798 the Tmprss2-Encoded Protease. *Molecular and cellular biology* **26**:965-975.
- 799 55. **Sales KU, Hobson JP, Wagenaar-Miller R, Szabo R, Rasmussen AL, Bey A, Shah MF,**
800 **Molinolo AA, Bugge TH.** 2011. Expression and Genetic Loss of Function Analysis of the
801 HAT/DESC Cluster Proteases TMPRSS11A and HAT. *PLoS one* **6**:e23261.

- 802 56. **Hemler ME.** 2005. Tetraspanin functions and associated microdomains. *Nature reviews.*
803 *Molecular cell biology* **6**:801-811.
- 804 57. **Dietrich C, Volovyk ZN, Levi M, Thompson NL, Jacobson K.** 2001. Partitioning of Thy-1,
805 GM1, and cross-linked phospholipid analogs into lipid rafts reconstituted in supported
806 model membrane monolayers. *Proceedings of the National Academy of Sciences* **98**:10642-
807 10647.
- 808 58. **Wang Y, Murakami Y, Yasui T, Wakana S, Kikutani H, Kinoshita T, Maeda Y.** 2013.
809 Significance of GPI-anchored protein enrichment in lipid rafts for the control of
810 autoimmunity. *Journal of Biological Chemistry.*
- 811 59. **Brown DA, London E.** 2000. Structure and Function of Sphingolipid- and Cholesterol-rich
812 Membrane Rafts. *Journal of Biological Chemistry* **275**:17221-17224.
- 813 60. **Gomez-Mouton C, Abad JL, Mira E, Lacalle RA, Gallardo E, Jimenez-Baranda S, Illa I,
814 Bernad A, Manes S, Martinez AC.** 2001. Segregation of leading-edge and uropod
815 components into specific lipid rafts during T cell polarization. *Proceedings of the National*
816 *Academy of Sciences of the United States of America* **98**:9642-9647.
- 817 61. **Charrin S, Manié S, Thiele C, Billard M, Gerlier D, Boucheix C, Rubinstein E.** 2003. A
818 physical and functional link between cholesterol and tetraspanins. *European Journal of*
819 *Immunology* **33**:2479-2489.
- 820 62. **Nomura R, Kiyota A, Suzaki E, Kataoka K, Ohe Y, Miyamoto K, Senda T, Fujimoto T.**
821 2004. Human coronavirus 229E binds to CD13 in rafts and enters the cell through caveolae.
822 *Journal of virology* **78**:8701-8708.
- 823 63. **Sun X, Whittaker GR.** 2003. Role for influenza virus envelope cholesterol in virus entry and
824 infection. *Journal of virology* **77**:12543-12551.
- 825 64. **Kawase M, Shirato K, van der Hoek L, Taguchi F, Matsuyama S.** 2012. Simultaneous
826 treatment of human bronchial epithelial cells with serine and cysteine protease inhibitors
827 prevents severe acute respiratory syndrome coronavirus entry. *Journal of virology*
828 **86**:6537-6545.
- 829 65. **Bahgat MM, Blazejewska P, Schughart K.** 2011. Inhibition of lung serine proteases in
830 mice: a potentially new approach to control influenza infection. *Virology journal* **8**:27.
- 831 66. **Owsianka AM, Timms JM, Tarr AW, Brown RJ, Hickling TP, Szejek A, Bienkowska-
832 Szewczyk K, Thomson BJ, Patel AH, Ball JK.** 2006. Identification of conserved residues in
833 the E2 envelope glycoprotein of the hepatitis C virus that are critical for CD81 binding.
834 *Journal of virology* **80**:8695-8704.
- 835 67. **Lee KK, Pessi A, Gui L, Santoprete A, Talekar A, Moscona A, Porotto M.** 2011. Capturing
836 a fusion intermediate of influenza hemagglutinin with a cholesterol-conjugated peptide, a
837 new antiviral strategy for influenza virus. *The Journal of biological chemistry* **286**:42141-
838 42149.
- 839 68. **Bosch BJ, Martina BE, Van Der Zee R, Lepault J, Haijema BJ, Versluis C, Heck AJ, De
840 Groot R, Osterhaus AD, Rottier PJ.** 2004. Severe acute respiratory syndrome coronavirus
841 (SARS-CoV) infection inhibition using spike protein heptad repeat-derived peptides.
842 *Proceedings of the National Academy of Sciences of the United States of America* **101**:8455-
843 8460.
- 844 69. **Lu L, Liu Q, Zhu Y, Chan KH, Qin L, Li Y, Wang Q, Chan JF, Du L, Yu F, Ma C, Ye S, Yuen
845 KY, Zhang R, Jiang S.** 2014. Structure-based discovery of Middle East respiratory syndrome
846 coronavirus fusion inhibitor. *Nature communications* **5**:3067.

847

Figure 1





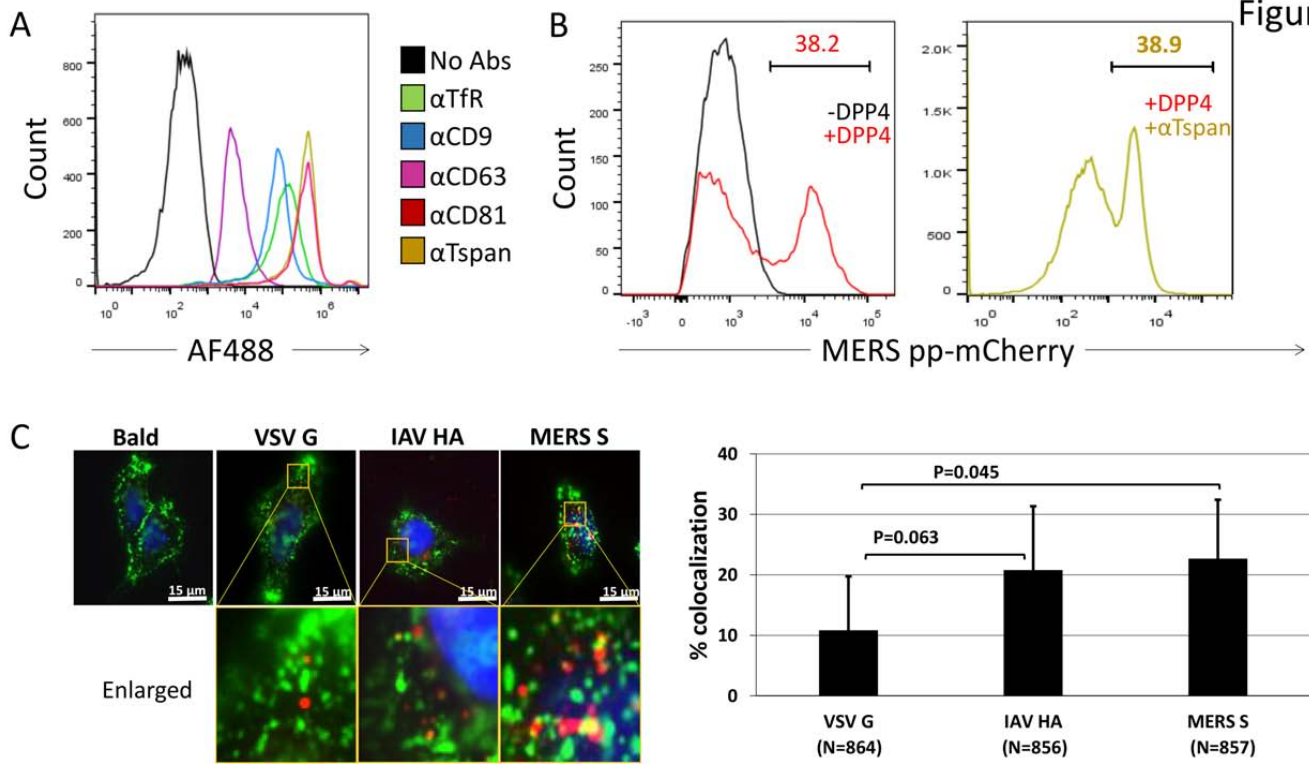


Figure 3

Figure 4

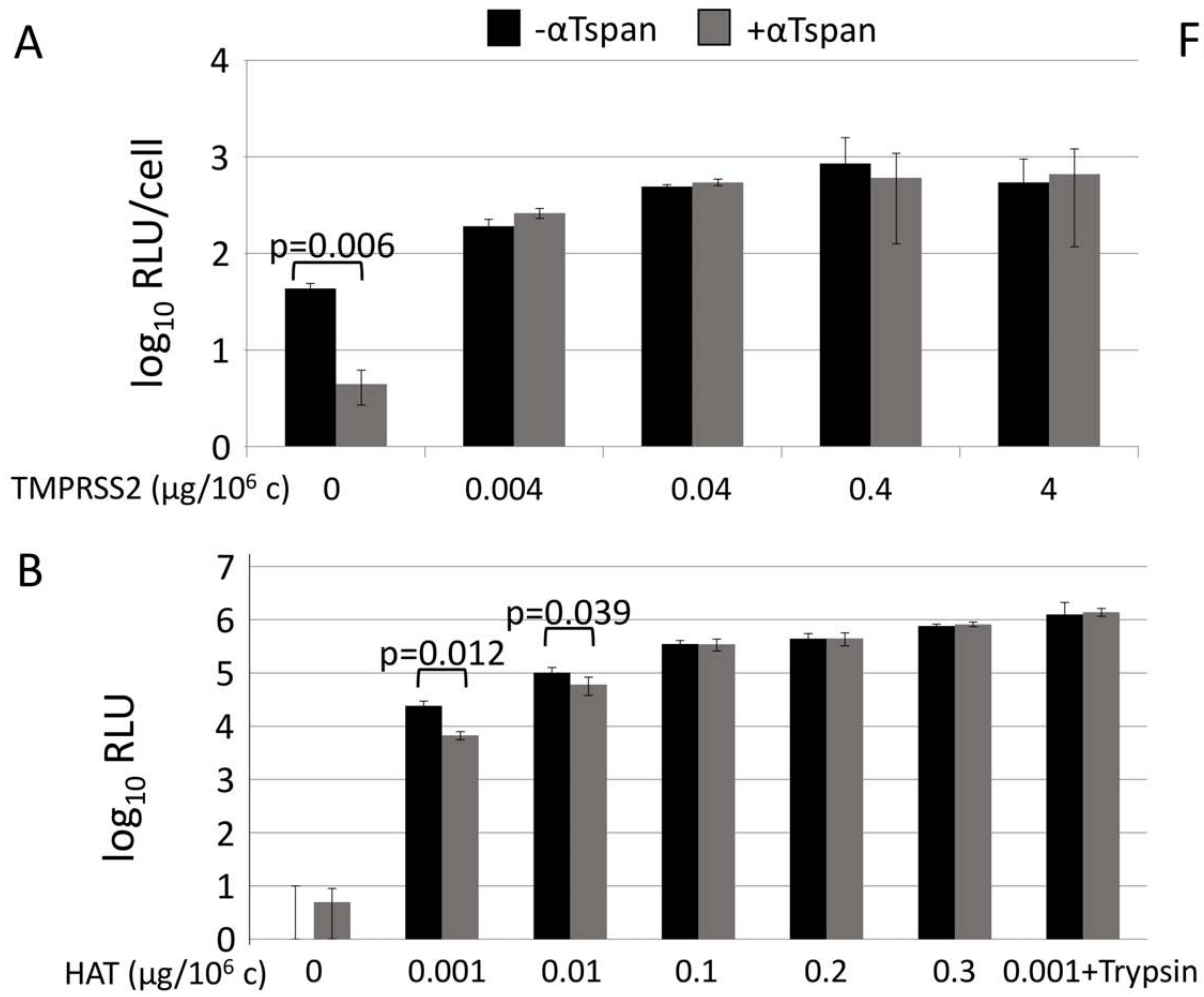
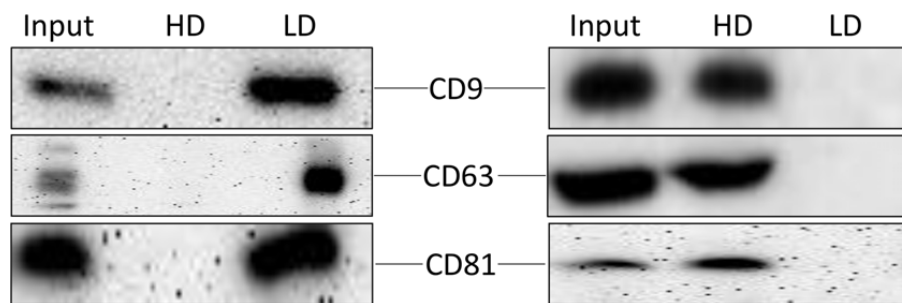
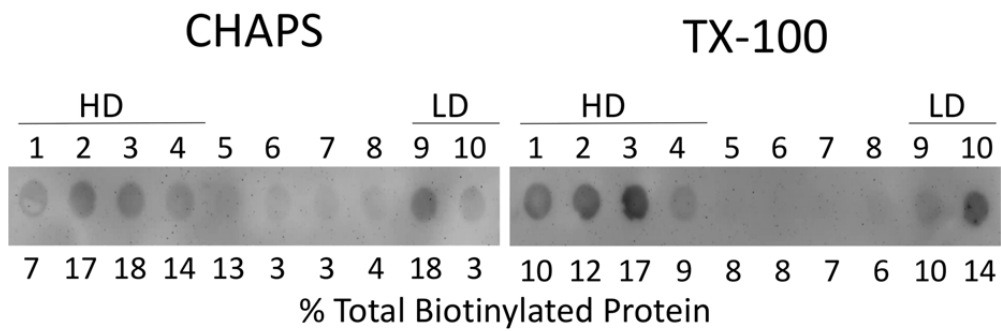
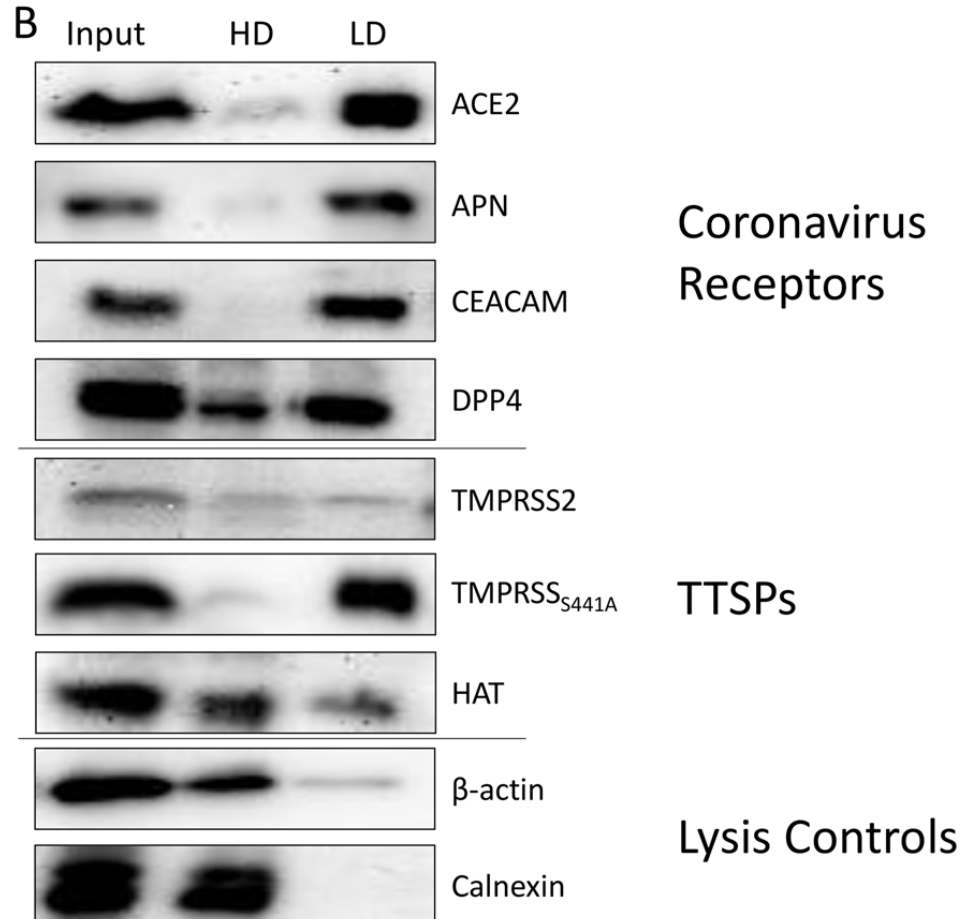


Figure 6

A



B



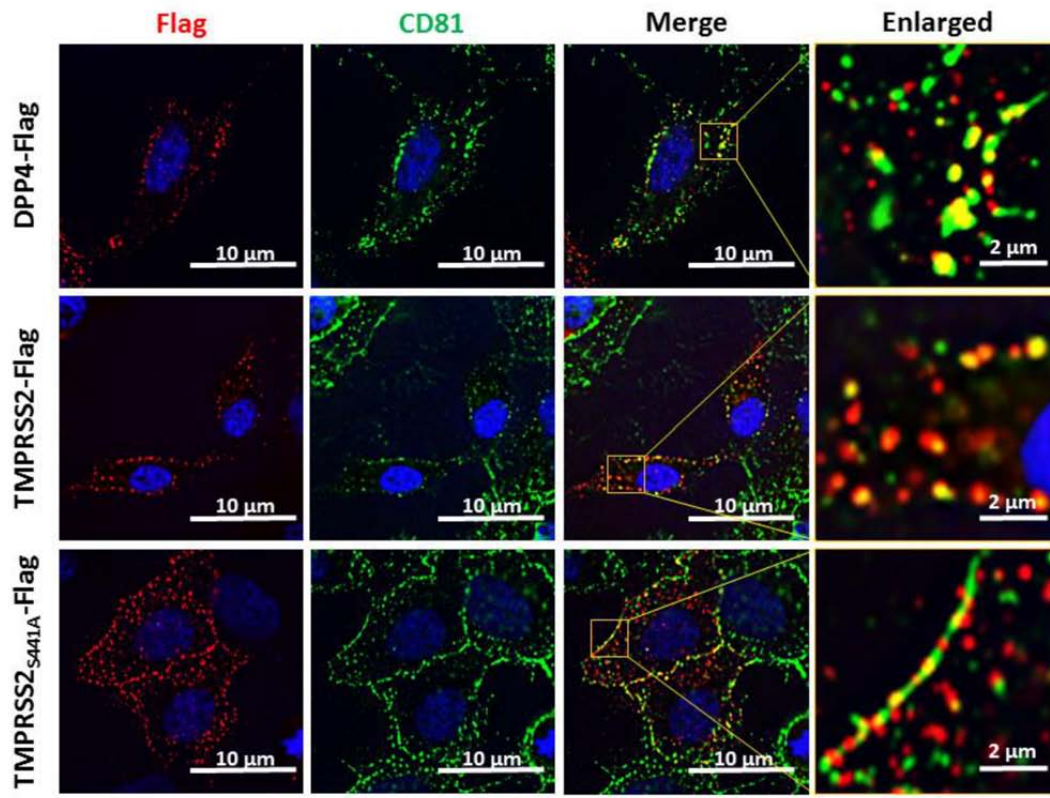


Figure 7

